Chapter 3
RF-Gun Design and Beam Dynamic Study

3.1 Introduction

An S-band thermionic cathode RF-gun has been designed as an electron source for producing femtosecond electron bunches at the SURIYA facility. The main advantage of a thermionic RF-gun is its higher current, higher brightness, lower emittance and higher electron beam energy compared to a conventional DC-gun. There is also no need for a complicate bunching system like in the DC-gun. Moreover, the operation of the thermionic cathode is simpler and cheaper than a photocathode. In addition, the thermionic cathode RF-gun exhibits essential features for efficient bunch compression. First, high acceleration to near relativistic energy at a few MeV (2-3 MeV) within a short distance allow space charge effects little time to dilute the beam emittance. Second, the energy-time phase space of the particle distribution produced in an RF-gun is suitable for simple and efficient bunch compression in an alpha magnet. Third, the particle density obtainable from a thermionic cathode can be increased to sufficient high values at which space charge effects become uncontrollable at low electron energies. The SURIYA RF-gun has been modified from the Stanford SUNSHINE RF-gun which has been originally designed for a different application not for producing femtosecond electron bunches. The design of the SURIYA RF-gun was specially optimized for magnetic bunch compression of a low energy electron beam and designed to produce femtosecond electron bunches at a desired experimental station.

3.1.1 RF-Gun Characteristics

SURIYA RF-gun is a thermionic RF-driven electron source consisting of one and a half resonant cavities with a side-coupling cavity. The first half-cell and the second full-cell are a π-mode standing wave RF-structures. Electromagnetic field is applied to the RF-gun via a rectangular waveguide input-port at the full-cell and the field in the two cells is coupled through a π-mode external side-coupling cavity. Hence, the whole RF-gun is represented by three coupled resonant

cavity operating in the $\pi/2$ excitation-mode. There is a phase-shift of 90^o between the half-cell and side-coupling cell, and between the side-coupling cell and the full-cell. Thus, the field in the half-cell and the full-cell are 180^o out of phase. A stainless steel tuning rod inside the side-coupling cavity is used to adjust the coupling and consequently the RF-power ratio of the two cells. The thermionic cathode is mounted at the center of the end wall of the first half-cell and does not affect the field inside the gun. Figure 4.1 illustrates the SURIYA RF-gun cross-section and 3D-view showing the two main RF-cavities with the side coupling cavity, the thermionic cathode, the RF-power input port and the beam-exit port.

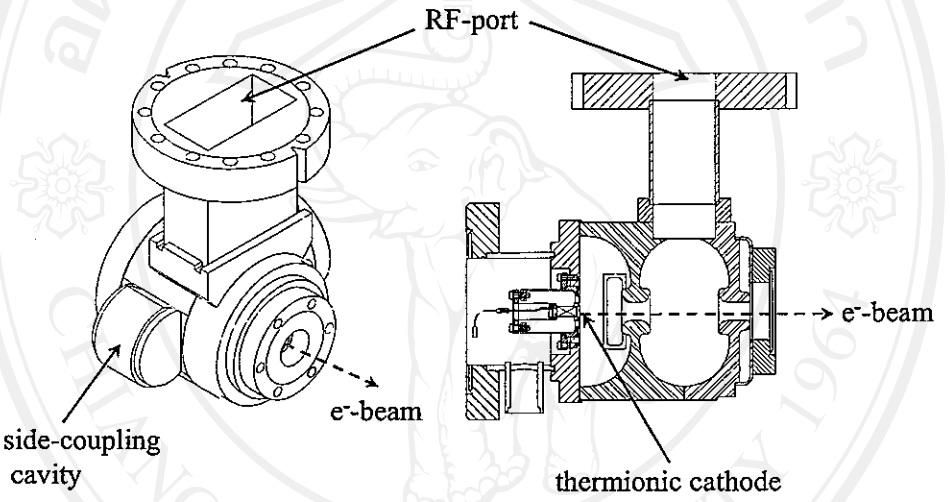

Figure 3.1. Cross-section and 3D-view of the SURIYA RF-gun.

In the thermionic cathode RF-gun, electrons are continuously emitted by the cathode but can only be extracted and accelerated during half an RF-cycle. Since the RF-gun is operated at 2856 MHz its operating cycle is about 350 ps. Electrons are emitted from the heated cathode with thermal energies of a few eV and are accelerated rapidly through the first half-cell when an RF-field is in the accelerating phase. Electrons with kinetic energies of about 0.5-0.6 MeV are accelerated out of the half-cell and enter into the second full-cell, while the fields in the full-cell reaches now the accelerating phase. Electrons are further accelerated through the full-cell resulting in a relativistic electron beam with a maximum kinetic energy of 2.0-2.5 MeV depending on the accelerating gradient in the two cells. Some fraction of electrons that are emitted late from the cathode feel a strong decelerating field in the half-cell and are decelerated to return and to hit the cathode causing additional cathode heating. This leads to back-bombardment

effect, which is one of the disadvantage of the thermionic RF-gun. Moreover, some electrons, that enter late in the second full-cell, feel also the decelerating field and return into the first half-cell and hit the cathode contributing to more back-bombardment effect. The details of this effect will be discussed experimentally in Chapter 6. Hence, to design the RF-gun, both the first and the second cell are required to be constructed such that most electrons are accelerated out of the gun. Energetic electrons that exit the RF-gun comprise the electron bunches with an energy-time correlation due to the time-varying nature of the RF-fields.

3.1.2 RF-Gun Numerical Simulations

In the RF-gun, electrons are emitted continuously from a thermionic cathode and are accelerated by the electromagnetic fields (RF-field) from thermal energies to relativistic energies with velocities approaching the speed of light in a very short distance. The continuous emission of the electrons from the cathode, the time-varying nature of the electromagnetic fields, the rapid acceleration from thermal velocities to relativistic velocities and the space-charge effect from Coulomb repulsion lead to a complicated analysis of the electron dynamics in the RF-gun. Therefore, numerical computer codes were employed to investigate the optimum geometric and electrical RF-parameters and study details of beam evolution in the RF-gun.

In the SURIYA RF-gun design, a code SUPERFISH [36] was used to optimize RF-parameters as well as to model RF-fields inside the RF-gun. SUPERFISH/POISSON is a well-established group code from the Los Alamos National Laboratory (LANL) that calculates frequencies and simulates electromagnetic field distributions for resonant cavity in two dimensions. This code allows the simulation of RF-cavity shapes and tuning to desired resonant frequency as well as to provide details of RF-parameters such as quality factor, cavity wall losses, shunt impedance etc. It also generates field distributions in the cavity for use by other particle-in-cell program like PARMELA [37]. PARMELA is a particle-in-cell code which can track many particles through the fields obtained from SUPERFISH. In PARMELA simulations, we assume that the cathode emits a uniform stream of discrete macroparticles (each of which represents many electrons) comprising an electron bunch at the RF-gun exit. The PARMELA study concentrate on simulations of a single-bunch evolving in the RF-cavities by solv-

ing Maxwell's equations for the electromagnetic field and in the presence of space charge forces acting on macroparticles. In our study, PARMELA was used to simulate the dynamics of macroparticles inside the RF-gun including space charge effects. PARMELA results show both longitudinal and transverse particle phase space distributions.

For beam transport and bunch compression system, additional codes Beam Optics [38] and Bunch Compression [39] are used to simulate beam optics and beam dynamics in the α-magnet, the linac and other components of beam transport line. In Beam Optics simulations the beam transport line was designed to optimize the beam sizes through the whole beam line. The magnets' field and the linac acceleration gradient obtained from this program can be used in beam dynamic studies with code Bunch Compression. The computer code Bunch Compression is used to simulate particle dynamics from the gun exit to the experimental station. Locations of the experimental station where the shortest bunch length is to be achieved as well as other useful parameters, for example, bunch charge and peak current can be determined using the code. In this chapter, results of simulations from SUPERFISH for the RF-gun design as it was built will be presented and discussed to give ideal RF-gun parameters and electromagnetic field distributions. The beam dynamic simulation results using the codes PARMELA, Beam Optics and Bunch Compression will also be discussed in this Chapter.

3.1.3 Comparison of Analytical and SUPERFISH Calculations

In this section some analytical calculations based on the information of the RF-gun parameter descried in Chapter 1 for a TM_{010} pillbox cavity resonating at 2856 MHz will be presented and compared with SUPERFISH simulations to demonstrate the validity of the code. In both, analytical calculations and simulations the average electric of 1 MV/m was used. The results from analytical calculations and from SUPERFISH simulations are compared in Table 4.5. There are slightly different values between both results may comes from the number of digits used in calculations and the mesh size in SUPERFISH simulations. The results of analytical calculation and SUPERFISH simulation are within 0.2 %. However, the RF cavity shape that we use in a real application is more complicated than the pillbox cavity. It will be very difficult to calculate every parameters

analytically. Hence, using a computer code such as SUPERFISH to simulate the cavity parameters is very useful and convenient for the RF-cavity design.

Table 3.1. RF-parameters for a pillbox cavity from analytical and SUPERFISH calculations.

Parameter	Calculation	SUPERFISH	% Different
RF frequency (MHz)	2856	2856.4	0.01
Cylindrical wall power loses (W)	175.40	175.24	0.08
Cap wall power loses (W)	67.13	67.05	0.12
Total wall power loses (W)	309.65	309.35	0.10
Specific shunt impedance (M/m)	169.50	169.68	0.18
Stored energy (mJ)	0.318	0.317	0.17
Unloaded Q-factor	18370	18402	0.11
Cavity filling time (μs)	1.024	1.025	0.10

3.2 RF-Simulations

The electromagnetic parameters of the RF-gun were simulated by using the code SUPERFISH. The simulations includes shape optimization, RF-parameter determination and accelerating field distribution. Since SUPERFISH is a 2D-simulation code its results are not accurate for the whole RF-gun. The RF-gun will have to be fine tuned during construction and low-level RF-measurements to get the desired resonant frequency. A convergence test has been done to ensure that mesh triangles are small enough for accurate field calculations. In our study the mesh size in both longitudinal and radial directions were chosen at 0.3 mm.

Since internal geometric features of the RF-gun cavities determine greatly the final beam characteristics the optimization of the RF-gun geometry is important in its design. The geometrical features can be separated into two groups; those which affect mainly RF-parameters and have little effect on beam parameters of interest and those which affect mostly beam characteristics. Figure 3.2 shows the cross-section of the half-cell and the full-cell with the electric field profile. The cavities are re-entrant type cavities with noses that protrude into the center maximizing the electric field amplitude along the axis for a given input RF-power. The cavity diameter determines the resonant frequency while the length of the effective cavity can be adjusted by the dimension a or the iris length by

varying dimensions c and e. The design of the RF-gun based on the the length of the full-cell is one-half of the RF-field wavelength. For electrons travel with velocities approach the speed of light ($\beta \approx 1$) in the 2856 MHz RF-field, the free space wavelength becomes $\lambda_{rf} = c/f = 10.5$ cm and the length of the full-cell in case of pillbox cavity should be about 5.25 cm. However, real cavity is not simple like the pillbox the cavity length must be adjusted to optimum value. In our RF-gun optimization, the physical length of the full-cell is 5.81 cm. The overall length of the gun is 9.02 cm and the maximum inner radius is 4.19 cm. The SURIYA RF-gun design has been started from the Stanford SUNSHINE RF-gun. There are two important changes that have been made for the new improved RF-gun design. First, a nose cone at the cathode plate of the SUNSHINE RF-gun, which introduced source of focusing while contributing to significant bunch lengthening, was replaced by a flat cathode plate to minimize the beam divergence. Second, the iris diameter at the cell ends are increased to reduce the radial electric fields resulting in less beam divergence at the gun exit. Comparison of the beam divergence of the SUNSHINE RF-gun and the new improved gun is shown in Sec.3.4.

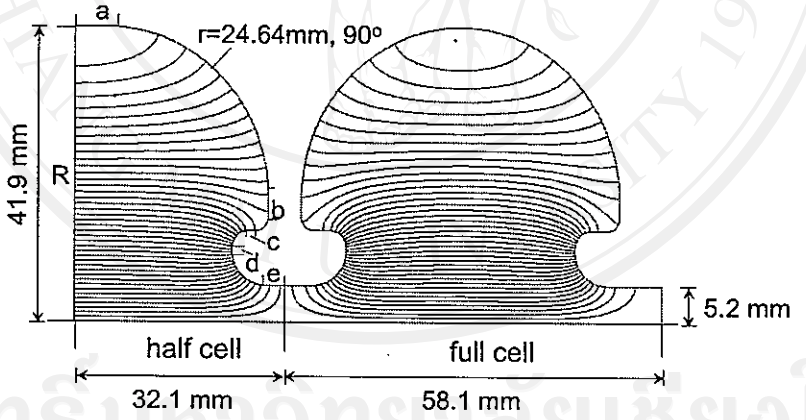

Figure 3.2. Internal RF-gun geometry and the electric field lines.

The geometry of the optimized SURIYA RF-gun used for simulations and for the actual gun as built are presented in Appendix A. It can be seen from the electric field contour that the half-cell and the full-cell is a π-excitation mode. The side coupling-cavity, not shown in the figure, leads the whole RF-gun to operate at the $\pi/2$-excitation mode. The normalized accelerating field profile along the longitudinal cross-section of the RF-gun is shown in Fig.3.3. The field in the first half-cell was chosen to be lower than the second full-cell so the back bombardment

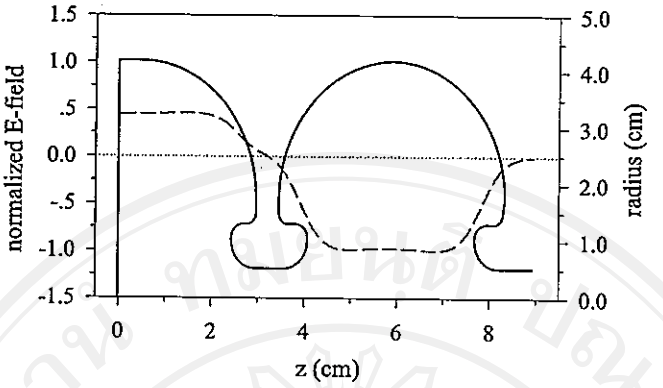

Figure 3.3. Axial electric field profile inside the RF-gun.

power at the cathode is less than the cathode heating power. This situation allows us to stabilize the RF-gun operation by a cathode feedback control. Some RF-parameters of the half-cell and the full-cell from SUPERFISH simulations are listed in Table 3.2. It should be noted that the cavity effective length is defined as the accelerating voltage divided by the peak accelerating field as expressed in (2.30)-(2.31).

Table 3.2. RF-parameters for the optimized RF-gun cavities from SUPERFISH simulations.

Parameter	Half-cell	Full-cell
RF frequency (MHz)	2863.6	2825.0
Velocity, $\beta = v/c$	0.6132	1
Shunt impedance of (MΩ/m)	120.3	93.1
Cavity length (mm)	32.1	58.1
Effective length (mm)	25.1	38.7
Unloaded Q-value	15263	13022
Peak to average field ratio (E_p/E_0)	2.30	2.85

3.3 Beam Dynamic Study

The code PARMELA is used to determine the dependence of expected beam characteristics on external parameters as well as on space charge forces. Unfortunately, the PARMELA cannot deal with particle beam dynamics in an α-magnet, thus an additional code Bunch Compression has been developed to

simulate the dynamics of particles travelling through the beam transport line downstream of the RF-gun including the α-magnet, quadrupole magnets, linac and some drift spaces. The beam dynamic studies described in this section concentrate on the RF-gun design before construction. However, some beam dynamic results for the actual RF-gun as built will be presented and compared to the design results later in the next section.

3.3.1 Numerical Beam Simulations of RF-Gun

PARMELA simulations were performed to investigate electrons beam dynamics inside the RF-gun including effects of space-charge forces. We assume that the cathode emits a uniform electron beam with a current of 2.9 A represented by 100,000 macroparticles per 2856 MHz RF-cycle. Each macroparticle represents a charge of 10.15 fCb equivalent to 6.34×10^4 electrons. The uniform current of 2.9 A corresponds to 285.6 macroparticles per picosecond at the cathode. At the gun exit we observe a much higher particle density during the first few picoseconds at the head of each bunch due to a time-varying field feature inside the RF-gun.

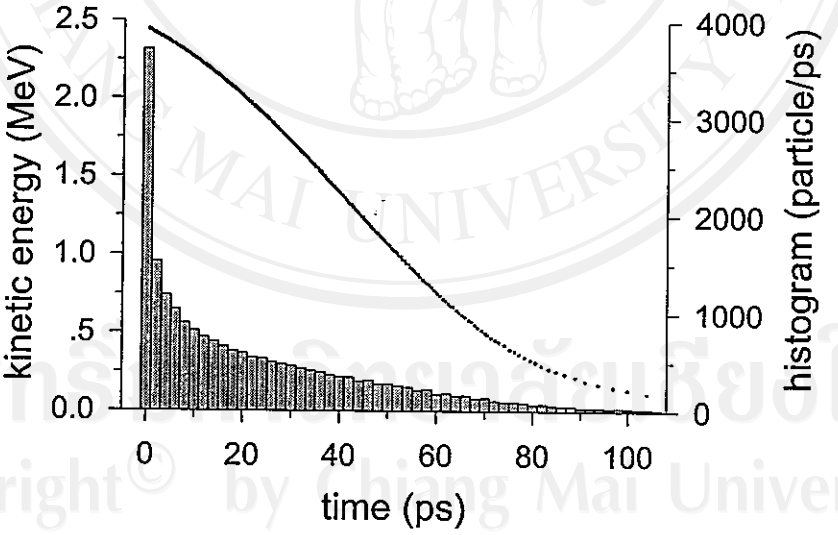

Figure 3.4. Particle distribution in energy-time phase space for a single S-band bunch at the RF-gun exit with histogram. The units of the histogram are macroparticles (each representing 6.34×10^4 electrons) per picosecond.

The histogram in Fig.3.4 shows the distribution in a bunch. The dynamics of the concentration in the bunch head derives from the temporal variation

(time-varying-field) of the microwave field. The first electrons emitted from the cathode and accelerated encounter initially only a very small field which increases as the electrons travel through the half-cell. Electrons emerging somewhat later from the cathode into the raising RF-field gain speed more quickly. They actually are able to partially catch up with the earlier electrons creating a higher particle density in the head of the bunch. Most particles concentrate within about 10 ps at the head of the bunch and this part of each bunch is used throughout in the beam dynamic studies. Although the electrons are generated as a continuous wave (CW) beam from the thermionic cathode, they eventually emerge from the RF-gun in bunches with the periodicity of the RF frequency. This results in a large energy spread in each electon bunch from maximum energy down to zero. The bunch that actually exits the RF-gun is about 100 ps long (about one fourth of the RF-cycle). The most high energy electrons are accumulated at the head of the bunch of about 10 ps forming the useful fraction of the electron bunch.

3.3.2 Bunch Compression

The concave shape of the phase space distribution in Fig. 3.4 matches especially well to bunch compression in an alpha-magnet (α-magnet) [25] shown in Fig. 3.5. In an α-magnet, the electron beam enters the magnet in the xz-plane at an angle of 49.29^o with respect to the magnet axis or yz-plane and follows a closed loop similar to the letter α to exit the magnet again exactly at the entrance point independent of the particle energy, yet in a different direction. The α-magnet is therefore an acromat, while the path length s of the particle trajectory in the magnet exhibits a large dispersion, depending on the particle momentum cp and magnetic field gradient g like $s \propto \sqrt{cp/g}$ [40]. In this magnet, lower momentum particles follow a shorter path than higher momentum particles. This feature make the α-magnet a convenient and simple bunch-compressor for low-energy beams. One may change the magnet strength and thereby the compression without changing the direction of the beam path outside the α-magnet. It is interesting to note that a larger compression is obtained for a weaker α-magnet strength because bunch compression of relativistic particles is mostly based on path length rather than velocity dispersion.

The phase space distribution of Fig. 3.4 rotates clockwise as the beam travels through the α-magnet. It is noted that the highest energy electrons in

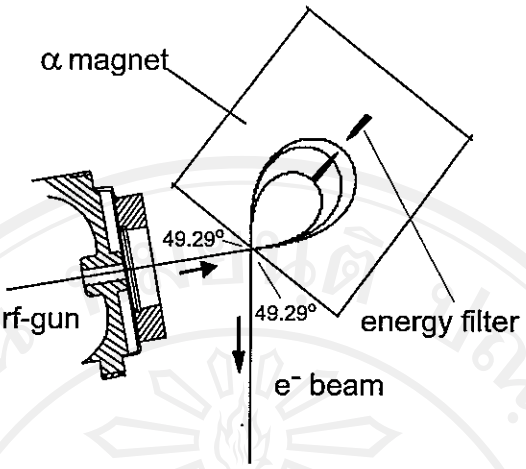

Figure 3.5. RF-gun and α-magnet schematic layout.

Fig. 3.4 exit the RF-gun first and follow a longer path through the α-magnet than lower energy electrons exiting the gun later. Even for moderately relativistic electrons, the velocity dispersion is small, although not negligible, and consequently lower energy electrons following a shorter path can catch up leading to bunch compression. Still, to avoid excessive bunch lengthening due to velocity dispersion which counteracts bunch compression, the beam energy should not be less than about 1 MeV and a short distance between RF-gun and α-magnet is desirable. Only the electrons at the head of the bunch that can be compressed and accelerated. An energy filter inside the α-magnet vacuum chamber, where the momentum dispersion is large, is used to select the desired part of the beam.

Downstream of the α-magnet, there may be a linear accelerator and/or some transport line guiding the beam to an experimental station. To compensate for the velocity dispersion, the value of the α-magnet field-gradient must be chosen such as to generate the shortest bunches at the desired experimental station. To obtain the shortest bunch at the experimental station, we need to overcompress the bunch such that the lower momentum particles exit the α-magnet first leaving higher energy particles behind as shown in Fig. 3.6. This phase space orientation together with the velocity dispersion due to the energy spread leads to the shortest bunch at the experimental station. This is a fortunate circumstance, since the bunch is most of the time long and the particle density low while the particle energy ahead of the linear accelerator is low and therefore space charge effects are minimized.

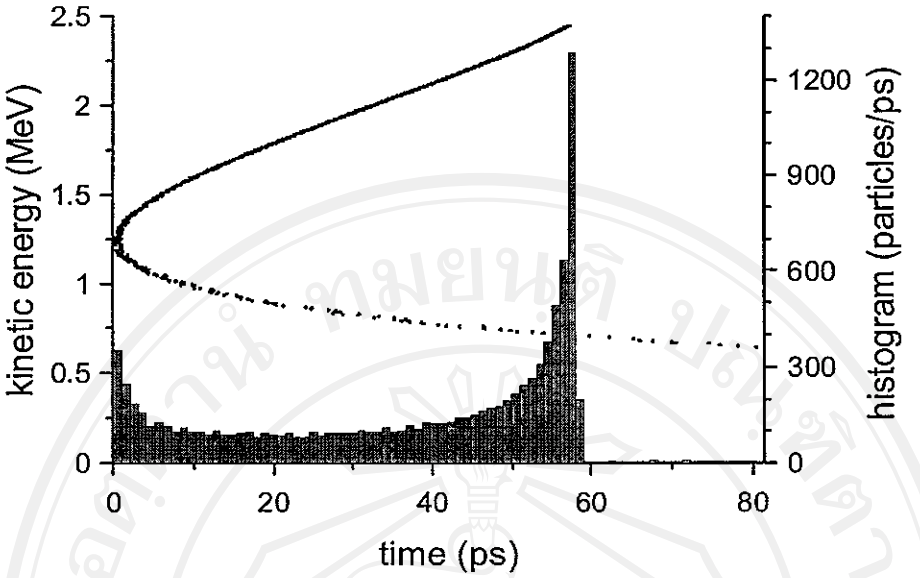

Figure 3.6. Particle distribution in energy-time phase space after the bunch compression in the α-magnet.

3.3.3 RF-Gun Field

The choice of the accelerating field in each cell of the RF-gun greatly controls the efficiency of bunch compression. In Fig. 3.7, we show the particle distribution in phase space at the RF-gun exit for different values of the accelerating fields in the half- and full-cell, respectively. The field ratio between the half- and the full-cell is kept constant to about 1:2 for this discussion. The field ratio is defined as a ratio of the peak accelerating field in the full-cell (E_{p2}) to the peak accelerating field at the cathode in the half-cell (E_{p1}) or $E_{ratio} = E_{p2}/E_{p1}$. In Fig.3.7 we note that particles in the bunch head are virtually quasi-monoenergetic for electric fields of about 45 MV/m in the half cell. This renders the beam unfit for bunch compression, yet exhibits a very desirable quasi-monochromatic beam to drive, for example, a Free Electron Laser. In this high field case, particles pass through the half-cell in less than one half RF-cycle and the integrated acceleration turns out to be about the same for particles emerging from the cathode during about the first 20 ps in the RF-cycle.

For lower fields, a monotonic correlation of particle energy with time appears as desired for bunch compression. In this situation, particles emerging at zero phase from the cathode will not quite reach the cavity exit before the field direction inverts and particles exiting the cathode at increasing RF-phases

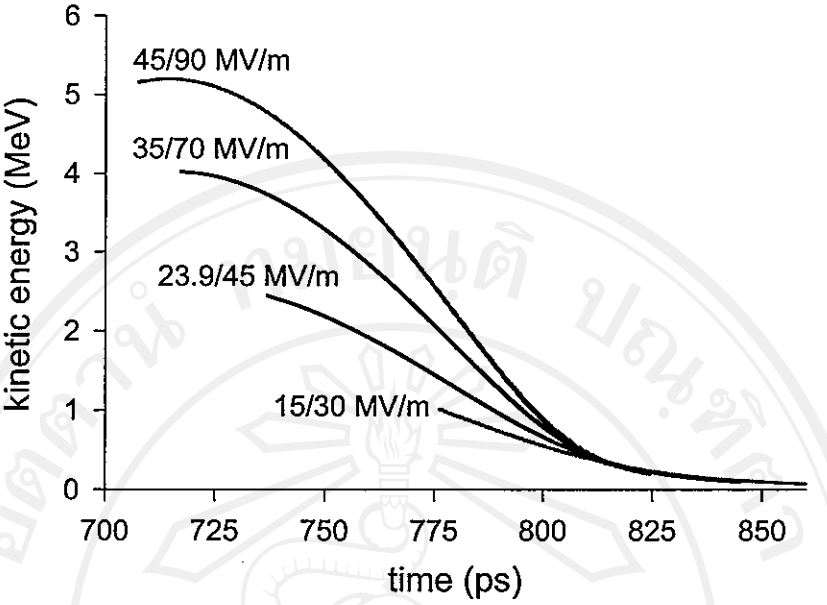

Figure 3.7. Particle distribution in energy-time phase space for different accelerating fields in the RF-gun.

experience increasing negative acceleration before they exit the half-cell. This becomes more true as the field is further reduced and is determined purely by cavity dimensions, RF-field amplitude and its temporal variation. At this point, we need to get some guidance on the choice of the electric field strength for optimum bunch compression. With the knowledge of the beam line downstream of the RF-gun, we may determine an ideally desired particle distribution at the gun exit.

3.3.4 Longitudinal Travel Time Formation

The beam transport line at SURIYA consists of the RF-gun, α-magnet, linac and some beam line components. Understanding of longitudinal travel time in each component of the beam transport line is required. To simplify the model for calculating the travel time in the beam transport line, we consider only the longitudinal coordinates. The BCompress code that we used in our study can also include transverse effects, arising from focusing elements. In this section, transverse effects are ignored. Electrons are generated from the thermionic cathode and accelerated out of the RF-gun with a large energy distribution from maximum energy to zero. From the gun exit, each electron travels through a drift

space (D_1) with travel time of

$$\Delta t_{D1} = \frac{D_1}{v_0} = \frac{D_1}{c\beta_0} = \frac{D_1}{c}\frac{E_0}{cp_0}, \tag{3.1}$$

where v_0 is the initial velocity of the electrons emerging from the RF-gun and cp_0 is the initial momentum which is related to the particle energy as $cp = \beta E = \beta(E_{kin} + mc^2)$. Downstream of the drift-space, particles travel through the α-magnet on a path length depending on the particle energy. Higher energy electrons travel in the magnet along a longer path than the lower energy electrons. This characteristic lets the lower energy particles leave the α-magnet earlier than the higher energy particles. The particle path length in the α-magnet is given by [40]

$$S = 191.65(cm)\sqrt{\frac{\beta\gamma}{g(G/cm)}}, \tag{3.2}$$

where g is the gradient of the α-magnet. Hence, the travel time through the α-magnet becomes

$$\Delta t_\alpha = \frac{S}{v_0} = \frac{191.65(cm)}{c\beta_0}\sqrt{\frac{cp_0}{g(G/cm)}}. \tag{3.3}$$

Following the α-magnet there is another drift-space (D_2) and the travel time of particle through this drift-space is

$$\Delta t_{D2} = \frac{D_2}{v_0} = \frac{D_2}{c}\frac{E_0}{cp_0}. \tag{3.4}$$

After the α-magnet and the drift-space, the particle enters the linac section. Since the particle velocity varies when it passes through the linac we must integrate the velocity along the length (L) of the linac and get

$$\Delta t_L = \int dt = \int_0^L \frac{dl}{v(l)}. \tag{3.5}$$

The particle velocity is given by

$$v(l) = c\beta(l) = c\sqrt{1 - \frac{1}{\gamma^2}} = \frac{c\sqrt{\gamma^2 - 1}}{\gamma}, \tag{3.6}$$

and the travel time through the linac becomes

$$\Delta t_L = \frac{1}{c}\int_0^L \frac{\gamma}{\sqrt{\gamma^2 - 1}}dl = \frac{mc^2}{cA}(\sqrt{\gamma_i^2 - 1} - \gamma_0^2 - 1) \tag{3.7}$$

The energy of a particle in the linac can be expressed as $E = \gamma mc^2 = mc^2 + E_{kin} + A \cdot l$, where A is the linac acceleration. Then, $\gamma_i = (mc^2 + E_{kin} + A \cdot l)/mc^2$ and $\sqrt{\gamma^2 - 1} = cp/mc^2$. Hence, the travel time of a particle through the linac is

$$\Delta t_L = \frac{1}{cA}(\sqrt{(E + A \cdot l)^2 - 1} - cp_0) = \frac{1}{cA}(cp_i - cp_0), \tag{3.8}$$

where cp_i is the momentum of particle after the linac acceleration. Downstream of the linac there is a drift-space (D_3) leading to the experimental station. The travel time through this drift-space is then

$$\Delta t_{D3} = \frac{D_3}{v_i} = \frac{D_3}{c}\frac{E_i}{cp_i}. \tag{3.9}$$

3.3.5 Ideal Phase Space Distribution

For a given beam transport line, an ideal electron phase-space distribution at the RF-gun exit can be defined. We need to establish a theoretically optimum bunch distribution and try to figure out how to achieve such a distribution. Comparison of the ideal phase space distribution with an actual electron distribution lets us determine the proper RF-gun field for producing the shortest electron bunches. Figure 3.8 shows the comparison of longitudinal phase-space distribution at the RF-gun exit and at the experimental station. As indicated in Fig. 3.8, the first particle to exit the RF-gun in each cycle at time $t_0 = 0$ is the reference particle, which also happens to be the particle with the highest momentum, and will arrive at the experimental station at time t_{ref}. An electron with lower momentum, exiting the RF-gun at a time δt later, travels to the experiment in a time Δt. For all particles to arrive at the experimental station at the same time, the travel time for the i^{th} particle must be

$$\Delta t(i) + \delta t(i) = t_{ref}, \tag{3.10}$$

where $\Delta t(i)$ is the travel time for the i^{th} particle travel from the RF-gun exit to the experimental station, t_0 is the time that the reference particle exits the RF-gun and $\delta t(i)$ is the time that the i^{th} particle exits the RF-gun. If the i^{th} particle, starting at time $\delta t(i)$ travels faster it can arrive at the experimental station simultaneously with the reference particle. Equation (3.10) is therefore the condition for perfect bunch compression. To get perfect bunch compression at the experimental station, all elements in the beam transport line need to be

included. For this simulation we use the beam transport line of Fig. 3.9. Note that the transverse effect from quadrupole magnets was not included in the simulation in Fig. 3.8. The travel time of the i^{th} particle from the RF-gun exit to the experimental station can be written as

$$\Delta t(i) = \Delta t_{D1} + \Delta t_{\alpha} + \Delta t_{D2} + \Delta t_{L} + \Delta t_{D3}, \tag{3.11}$$

where $\Delta t_{D1}, \Delta t_{\alpha}, \Delta t_{D2}, \Delta t_{L}$ and Δt_{D3} are the travel time of the i^{th} particle through the beam transport line in Fig. 3.9 and can be calculated from the formulation in the previous section. Hence, the travel time of the i^{th} particle can be expressed as

$$\Delta t(i) = \frac{D1}{c}\frac{E_{0i}}{cp_{0i}} + \frac{191.65}{c\beta_{0i}}\sqrt{\frac{cp_{0i}}{g}} + \frac{D2}{c}\frac{E_{0i}}{cp_{0i}} + \frac{1}{cA}(cp_i - cp_0 i) + \frac{D3}{c}\frac{E_i}{cp_i}. \tag{3.12}$$

To get ideal bunch compression, the α-magnet gradient in (3.12) must be adjusted such that $\Delta t(i) + \delta t(i) = t_{\text{ref}}$. Calculating the ideal gun exit-times δt for all particle momenta, we get the ideally desired particle phase space distribution at the RF-gun exit as shown in Fig. 3.10 in comparison with an actual particle distribution.

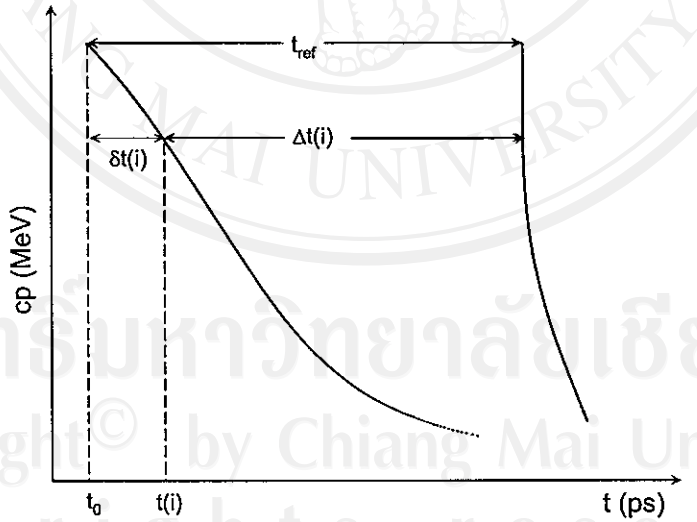

Figure 3.8. Comparison between longitudinal phase space distribution at the RF-gun exit (left curve) and at the experimental station (right curve).

The distribution within the bunch head of the ideal distribution in Fig. 3.10 has the same convex curvature as those we observe in Fig. 3.4. A proper

choice of the electric field strength can therefore match the actual to the ideal distribution at least over a finite range of particle energies. For too low energy particles, both distributions diverge greatly because particles travel too slow to be able to catch up. The range of almost perfect match extends over about the first 10 to 15 ps of each bunch where most of the charge is concentrated. A similar, but much smaller dynamic effect occurs in the second, full-cell cavity and must therefore be included as a correction in the overall optimization procedure. Close to ideal phase space distributions can be achieved if the accelerating field

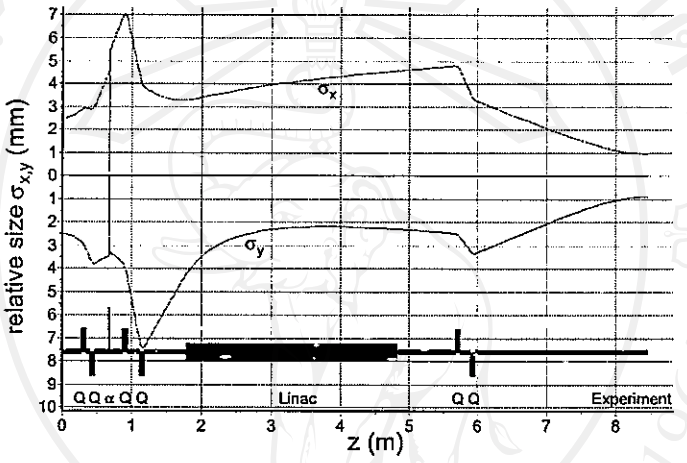

Figure 3.9. Beam transport line from RF-gun to experimental station (QF1-QD1-QF2-α magnet-QF3-QD2-linac-QF4QD3). (Note: α-magnet is shown as a thin element.)

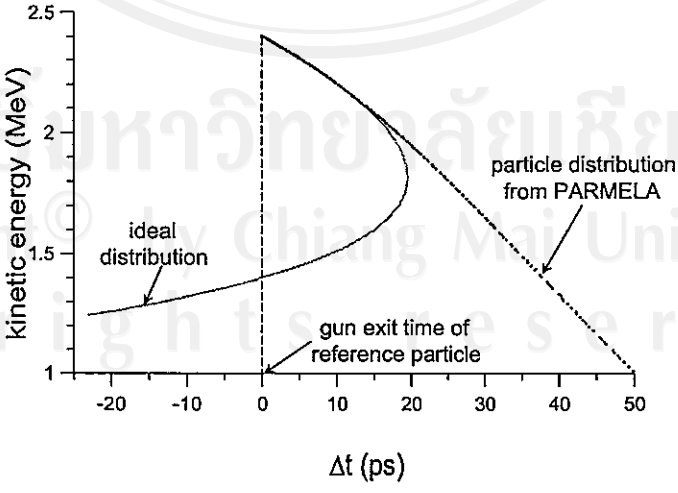

Figure 3.10. Ideal distribution and particle distribution from PARMELA simulation at the RF-gun exit.

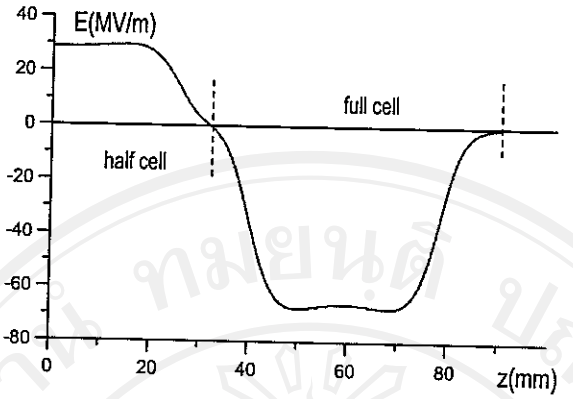

Figure 3.11. Axial electric field profile for optimum accelerating field ratio in the half-cell and the full-cell.

and length of the half-cell cavity is such that the reference particle can traverse its effective part within one half RF accelerating-period. For the RF-gun under discussion this optimization leads to a perfect match if the average accelerating field in the half-cell and in the full-cell are 23.9 and 45 MV/m, respectively. The electric field profile along the cavity axis in both cells is shown in Fig. 3.11.

3.3.6 Beam Dynamic Simulations at Experimental Station

The numerically simulated particle distribution of Fig. 3.4 is shown in Fig. 3.12 after compression and acceleration in the linear accelerator to 24 MeV. Note that the temporal particle distribution is shown with respect to the initial momentum at the RF-gun exit. The particle distribution in phase space and the histogram exhibit some characteristics which we will discuss in more detail. The beam transport line used in this study is shown in Fig. 3.9 and has been designed for minimum bunch length broadening due to path length dispersion. While this is not the only solution possible, we use it as an example to demonstrate the dynamics of the electron beam. The lattice parameters for this transport line are compiled in Table 3.3. A discontinuity of the beam size appears at the α-magnet because the beam size within the α-magnet can not be determined with available programs due to the large energy spread of particles in the magnet. Special care was taken in the design of this transport line to avoid any unnecessary focusing which could lead to path length dispersion as described later. For the design of the beam line shown in Fig. 3.9 we were able to reduce these effects to a negligible

level within the statistical fluctuations of bunch length due to the limited number of particles in the simulation.

Table 3.3. Optimized beam line lattice.

#	Name	l(m)	strength	units
1	D1	0.283		m
2	QD1	0.073	18.750	$1/m^2$
3	D3	0.050		m
4	QF2	0.073	-34.440	$1/m^2$
5	D4	0.200		m
6	$\alpha-$ magnet	n/a	399.00	G/cm
7	D5	0.189		m
8	QF3	0.073	43.300	$1/m^2$
9	D6	0.164		m
10	QD2	0.073	-39.717	$1/m^2$
11	D7	0.600		m
12	Linac	3.040	8.0	MeV/m
13	D8	0.853		m
14	QF4	0.073	19.664	$1/m^2$
15	D9	0.150		m
16	QD3	0.073	-21.623	$1/m^2$
17	D10	2.480		m

The phase space distribution of Fig. 3.12 represents the result of an optimization study which we will use in this section as a reference for more detailed discussions. It shows the particle distribution at the end of the beam line which is the location of optimum bunch compression (Fig. 3.9). Bunch lengthening due to path length dispersion caused by focusing in the beam transport line has been kept to a minimum in the particular design of the beam transport line (Fig. 3.9) and shows up as a small broadening of the Gaussian tails. The most obvious feature of the particle distribution is the oscillatory variation in time. This oscillation is believed to be caused by a shock wave instability caused by the sudden increase in the charge intensity at the head of each bunch [41]. That leads to an oscillatory

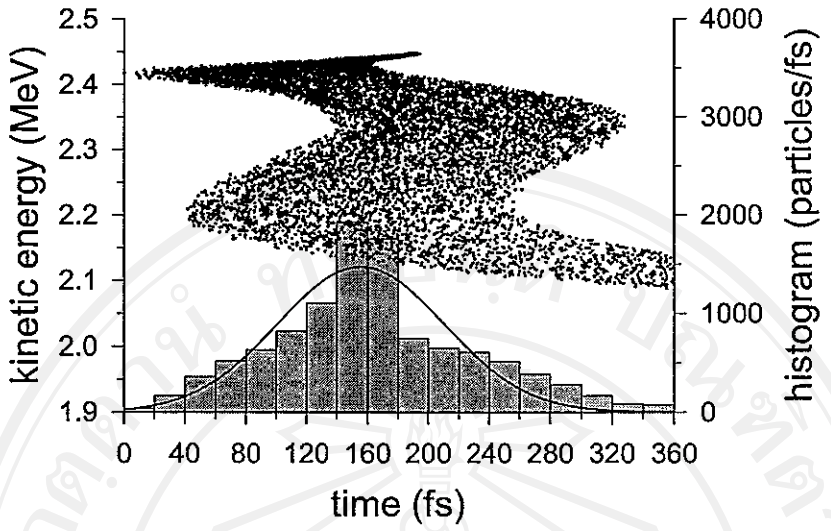

Figure 3.12. Particle energy-time phase space distribution after bunch compression and transport to the experimental station with histogram. The histogram can be fitted by a Gaussian with a standard width of 53 fs and a charge of 94 pCb.

of energy due to space charge forces along the bunch which in turn gives rise to temporal oscillations after compression in the α-magnet. This effect is expected to ultimately limit the bunch compression of low energy beams. This perturbation is established in the first half cell persisting over a few oscillations. When space charge forces are ignored, this instability does not appear and the longitudinal phase space is determined only by cathode geometry, RF focusing and thermal energy distribution. From the temporal oscillations of about ± 50 fs we derive a relative momentum ripple of $\pm 10^{-4}$. The expected bunch length, including transverse path length dispersion, is 53 fs rms at a total charge of 94 pCb. Some of the main beam characteristics from this optimized RF-gun are compiled in Table 3.4.

3.4 Transverse Particle Dynamics of RF-Gun

Due to the natural divergence of the beam and under the forces of focusing elements, particles follow trajectories which are oscillatory about the ideal beam axis and therefore longer than on-axis trajectories leading to path length dispersion. The RF-gun used in the SUNSHINE facility creates a large beam

Table 3.4. Optimized S-band RF-gun and beam parameters.

Parameter	Values	Unit
max.beam momentum, cp	2.91	MeV
velocity, $\beta = v/c$	0.9851	
Avg./max. field in half-cell	23.9/29.9	MV/m
Avg./max. field in full-cell	45.0/67.6	MV/m
Avg. field ratio (E_2/E_1)	1.88	
Max. field ratio (E_{p2}/E_{p1})	2.26	
Cathode emission current	2.9	A
Cathode radius	3.0	mm
Current density	$\sim$10	A/cm^2
Charge/bunch	94	pCb
Peak current	707	A
Bunch length, rms	53	fs
Norm.beam emittance, rms	3.8	mm-mrad

convergence/divergence as shown in Fig.3.13 which must be compensated with quadrupole focusing between RF-gun, α-magnet and experimental station. The slopes of particle trajectories being of the order of 10 mrad cause a significant spread of the path lengths and thus limit the shortest bunch achievable to about 120 fs [4].

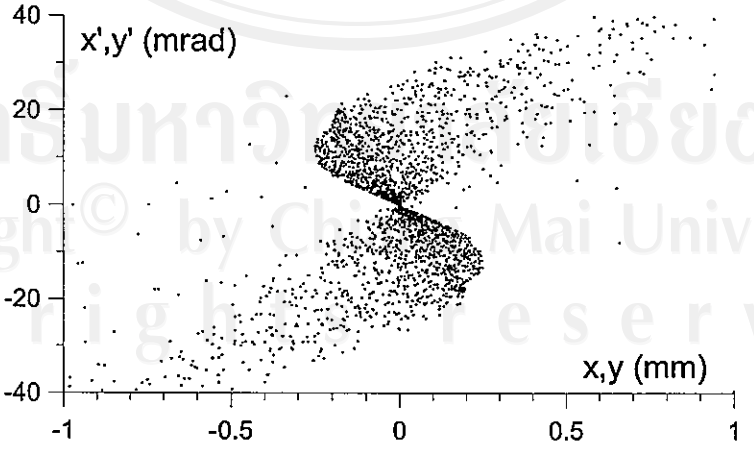

Figure 3.13. Transverse phase-space distribution at the exit of the SUNSHINE RF-gun (without space charge effects).

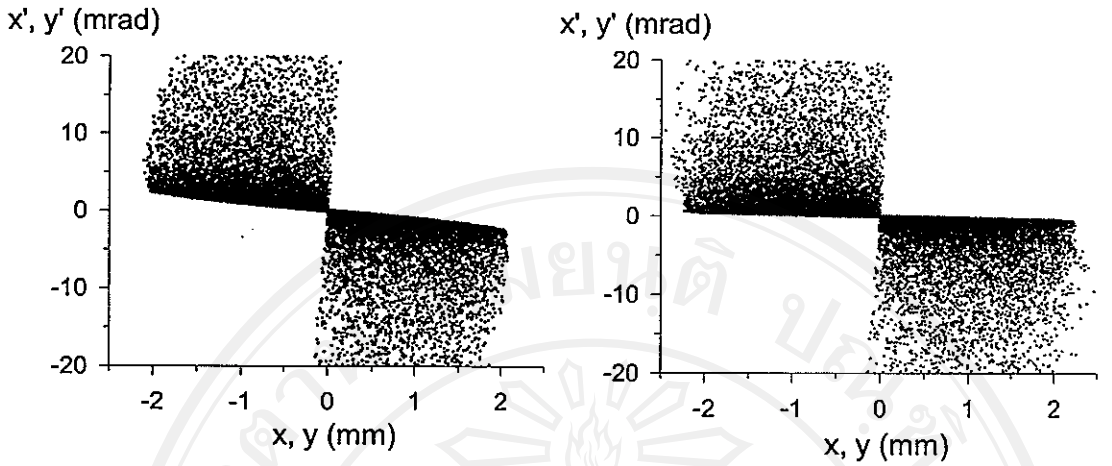

Figure 3.14. Transverse phase-space distribution of optimized RF-gun without (left) and with (right) space charge effects.

In the optimized SURIYA RF-gun design a flat cathode plate is used and the iris radii are increased to reduce the effect of radial RF-fields in their vicinity. Both changes result in a much reduced beam divergence as shown in Fig.3.14 (right) compared to the case for the SUNSHINE RF-gun shown in Fig.3.13. Ignoring space charge effects, a slightly convergent beam is desired (Fig.3.14, left) which then becomes a parallel beam (Fig.3.14, right) when repelling space charge forces are included. Bunch lengthening depends quadratically on the beam divergence and is therefore greatly reduced for the optimized gun design with less than 1 mrad of divergence for the core of the beam. Unfortunately, the α-magnet introduces strong focusing which must be matched by some external quadrupole focusing causing an unavoidable finite amount of bunch lengthening. This has been included in the simulation of the particle distribution of Fig. 3.12 for the transport line in Fig. 3.9.

To calculate the beam emittance, we take only the useful part of the beam with particle momenta of $cp \geq 2.60$ MeV (Fig. 3.12). Using the definition $\epsilon_{\rm rms} = \sqrt{\langle x^2 \rangle \langle x'^2 \rangle - \langle xx' \rangle^2}$ the useful beam rms emittance is $\epsilon_{\rm rms} = 0.69$ mm-mrad. For an average value of the kinetic energy of 2.35 MeV, $\beta\gamma = 5.51$ and the normalized beam emittance is $\epsilon_{\rm n,rms} = 3.8$ mm-mrad.

Since the cathode for the RF-gun is the thermionic cathode which electrons are emitted from the cathode by the heating power a thermal emittance of electrons as they are extracted from the cathode surface should be considered.

The normalized thermal cathode emittance, $\epsilon_{n,therm}$, from a uniformly emitting thermionic cathode of radius r_c and operating temperature T is given by [34]

$$\epsilon_{n,therm} = 2r_c\sqrt{\frac{kT}{mc^2}}, \tag{3.13}$$

where r_c is the cathode radius, k is the Botzmann constant ($k = 8.617 \times 10^{-5}$ eV/K) and mc^2 is the electron rest mass energy (0.511 MeV). The normalized thermal cathode emittance at $T \approx 1300\ K$ and a cathode radius of 3 mm is $\epsilon_{\text{n, therm}} = 0.28$ mm-mrad and it has been included in the PARMELA simulations.

3.4.1 Effect of Cathode Size

The size of the cathode diameter can limit the shortest achievable bunch length. Particles emerging at the same time from different cathode radii will travel through regions containing different radial field components. As a consequence, the length of the trajectories for particles emerging from different parts of the cathode at the same time differ although the particle kinetic energies at the RF-gun exit are almost the same. Such particles cannot be distinguished energetically and therefore resist bunch compression, thus limiting the shortest achievable bunch length.

Reducing the cathode diameter, space charge effects become increasingly evident. An intense pencil beam line in Fig.3.4, for example, does not remain thin during acceleration in the RF-gun if space charge forces are included. With decreasing cathode diameter and constant emission current, space charge forces from the bulk of the bunch accelerate particles in the head of the bunch to an undesirable degree. As a consequence, the bunch head follows a longer path in the α-magnet and the time distribution of the bunch head is tilted towards later times with respect to the rest of the bunch. Such a distribution cannot be compressed effectively. The choice of an emission current of 2.9 A from a 6 mm diameter cathode seems to be optimum while avoiding such problems. A cathode current of 2.9 A from a 6 mm diameter cathode relates to a current density of

$$j = \frac{I}{\pi r_c^2} = \frac{2.9\ A}{\pi(0.3\ cm)^2} \approx 10\ A/cm^2. \tag{3.14}$$

3.4.2 Beam Emittance and Particle Energy

The particle phase space distribution from an RF-gun has the familiar *butterfly-shape* due to time dependent focusing in the RF-field as evident from Fig.3.14 [42]. If high bunch intensities are desired, a commensurate increase of the overall beam emittance must be accepted. Closer inspection of the particle phase space distribution in other dimensions reveals, however, a significant amount of correlation with particle energy. In Fig.3.15 we show again the results of Fig.3.14(right) but this time including the finite effect of the thermal cathode emittance. Furthermore, we plot the transverse phase space distribution only for select energy bins of $\pm 0.5\%$ to show clearer the correlation. Since particles of different energies are also separated in time, this correlation provides an opportunity for emittance compensation. The unnormalized slice-emittances for 95% of the beamlet intensities including (ignoring) thermal cathode emittance are $\epsilon = 0.35(0.11), 0.42(0.21)$, and $0.45(0.34)$ mm-mrad for the 2.44, 2.36 and 2.29 MeV beamlets, respectively, as shown in Fig. 3.15.

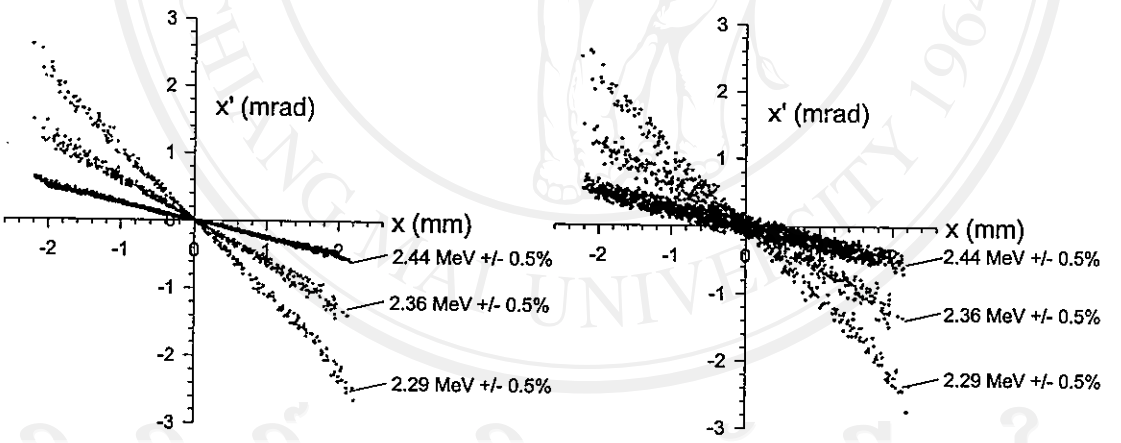

Figure 3.15. Transverse phase-space distribution of optimized RF-gun without (left) and with (right) space charge effects.

3.4.3 Schottky Effect

The presence of a strong field at the cathode will lower the work function of the cathode material due to the Schottky Effect (as described in Chapter 2). Let $E = E_0 \sin \omega t$ be the accelerating electric field on the cathode surface, with a maximum electric field E_0 and frequency $\omega = 2\pi f$. Then, Richardson's law with

Schottky correction may be expressed by

$$\frac{j}{AT^2} = exp[\frac{-e(\Phi_w - 0.012\sqrt{E_0 \sin \omega t})}{kT}. \tag{3.15}$$

In the RF-gun design, the average electric field in the half-cell, which has the cathode attached at the end wall of the half-cell is 23.9 MV/m and it represent the average field at the cathode surface. We consider a dispenser cathode with a work function of 1.2 eV when heated to about 1000^oC. By using the peak electric field at the cathode of 28.8 MV/m at 2856 MHZ, the maximum current density (j/AT^2) of thermionic emission from the cathode during the first 50 ps is shown in Fig 3.16 and it reveals that a higher heating temperature provides a higher current density of the electron beam. Relation of time versus j/AT^2 shows that the current density in term of j/AT^2 increases with time due to the characteristics of the time-varying RF-fields, which is applied to the gun cavity. During the course of a quarter period of the electric field the current density increases by about 20 %. For the SURIYA RF-gun we are interested mainly in the electron beam emitted during the first 20 ps where the variation of the emitted electron beam is about 10 %. This small variation seems to justify the assumption of a constant emission current of the thermionic cathode in PARMELA simulations.

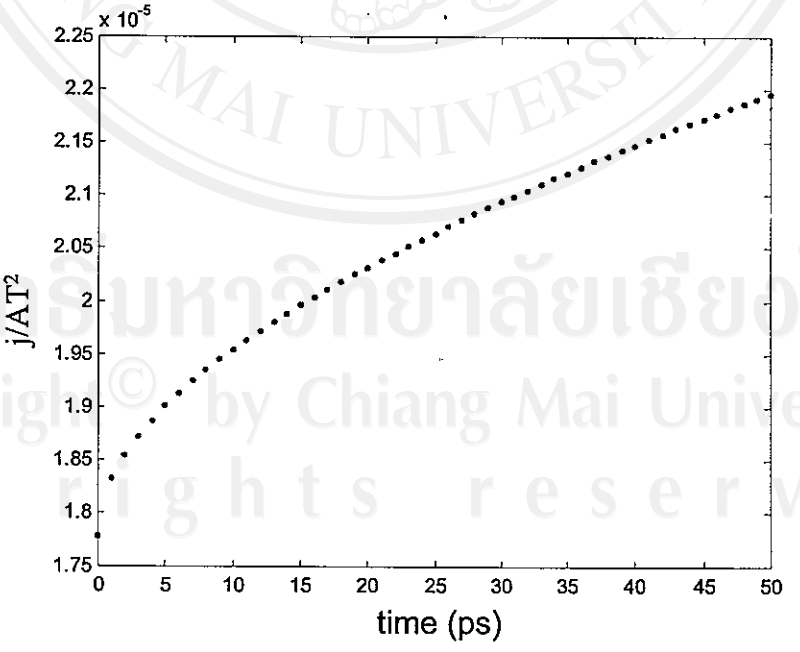

Figure 3.16. Relation of current density and time from Richardson's law with Schottky's correction.

3.5 Parameters and Beam Dynamic Results for SURIYA RF-Gun

The SURIYA RF-gun was constructed followed the SUPERFISH and PARMELA results. Based on a 2D-simulation, SUPERFISH can not be used to include 3D-shape, i.e, a coupling cavity, an RF-input port and a vacuum pumping port into the simulation. This leads to a deviation of the simulated results from the measured values which obtained in a low-level RF-measurements as discussed in Chapter 4. The actual dimensions of the RF-gun after the resonant frequency tuning were different from the design version describing in Sec.3.2. The actual RF-gun dimension is shown together with the design dimension in Appendix A. The SUPERFISH simulations were performed for the actual dimension RF-gun for the operating temperature of 27.5°C and the RF-parameters are complied in Table 3.5. The beam dynamics for this actual gun with the optimized beam line in Fig. 3.9 has been studied with the accelerating field amplitudes in the half-cell and the full-cell of 22.7 and 46.9 MV/m, respectively. The α-magnet gradient was adjusted to achieved the shortest bunch length at the experimental station of the beam line in Fig. 3.9. Beam dynamic study results are shown in Table 3.6.

Table 3.5. RF-parameters for the actual RF-gun cavities from SUPERFISH simulations.

Parameter	Half-cell	Full-cell
RF frequency (MHz)	2880.65	2868.77
Shunt impedance of (MΩ/m)	123.71	96.56
Cavity length (mm)	31.6	57.2
Effective length (mm)	24.9	39.2
Unloaded Q-value	15692	13343
Peak to average field ratio (E_p/E_0)	2.24	2.71

Although, the beam transport components of SURIYA beam line were installed following the optimized beam line but with the limitation of area and the components dimensions some beam line in Fig. 3.9 component positions are different from the optimized design. This leads to less efficient bunch compression at the experimental station. Details of the beam line components at SURIYA with the component parameters are complied in Table 3.7. The linac acceleration for this optimized beam line is the maximum acceleration that can be reached from the available RF-power at SURIYA. The optimization of the bunch compression

for the SURIYA RF-gun and actual beam line shows that the electron bunch length of 62 fs with the bunch charge of 94 pC and the peak current of 604 A can be expected.

3.6 RF-Power Requirements

Current and energy of an electron beam from the RF-gun depends on two factors; a current density of electron emitted from the cathode and an amount of RF-power applying from an external RF-source. Electrons are emitted from the cathode and are accelerated by accelerating electric fields inside the RF-cavity. The RF-power from external RF-source is required to be sufficient high for a beam loading power (P_{beam}). The energy conservation states that [40]

$$\frac{dU}{dt} = P_f - P_r - P_{cy} - P_b, \tag{3.16}$$

where U is the energy stored in the resonant cavity, P_f is the forward RF-power applying to the cavity, P_r is the reflected RF-power from the cavity, P_{cy} is the RF-power dissipated in the cavity wall and P_b is the beam power.

At the equilibrium state, the RF-fields inside the resonant cavity are constant and there is no stored energy change in the cavity (dU/dt=0). Then, the

Table 3.6. Beam parameters of SURIYA RF-gun with the beam line in Fig. 3.9.

Parameter	Values	Unit
Max.beam momentum, cp	2.904	MeV
Velocity $\beta = v/c$	0.6074	1
α-magnet gradient	398	G/cm
Avg./max. field in half-cell	22.7/28.7	MV/m
Avg./max. field in full-cell	46.9/68.5	MV/m
Avg. field ratio (E_2/E_1)	2.07	
Max. field ratio (E_{p2}/E_{p1})	2.39	
Cathode emission current	2.9	A
Cathode radius	3.0	mm
Current density	~10	A/cm^2
Charge/bunch	94	pCb
Peak current	682	A
Bunch length, rms	55	fs

Table 3.7. Beam line lattice for SURIYA system.

#	Name	l(m)	strength	units
1	D1	0.309		m
2	QD1	0.077	18.000	$1/m^2$
3	D3	0.037		m
4	QF2	0.077	-10.000	$1/m^2$
5	D4	0.200		m
6	$\alpha-$ magnet	n/a	410.00	G/cm
7	D5	0.305		m
8	QF3	0.077	55.650	$1/m^2$
9	D6	0.043		m
10	QD2	0.077	-58.860	$1/m^2$
11	D7	0.521		m
12	Linac	3.040	7.77	MeV/m
13	D8	0.801		m
14	QF4	0.078	35.272	$1/m^2$
15	D9	0.078		m
16	QD3	0.078	-40.590	$1/m^2$
17	D10	0.942		m

cavity wall losses becomes

$$P_{cy} = P_f - P_r - P_b. \tag{3.17}$$

The forward and reflected powers can be obtained from the high RF-power measurements (will be discussed in Chapter 6). The beam power P_b can also be obtained experimentally. In case of a coupled-RF system with an RF-coupling coefficient β_{rf}=1, there is no reflected RF-power. Therefore, the input RF-power from the klystron should be at least

$$P_f = P_{cy} + P_b. \tag{3.18}$$

3.6.1 Cavity Wall Losses

The average accelerating field in the half-cell and the full-cell that provides the best compression results (as described in Sec.3.3) is 23.9 and 45 MV/m.

The cavity power losses (P_{cy}) can be calculated from (2.43) and (2.31)

$$P_{cy} = \frac{V_{cy}^2}{r_s d} = \frac{E_{ave}^2 d}{r_s}, \tag{3.19}$$

where V_{cy} is the accelerating voltage, E_{ave} is the average accelerating amplitude, d is the cavity effective length and r_s is the specific shunt impedance of the cavity. From the SUPERFISH simulation results, the effective length of the half-cell and the full-cell is 2.51 and 3.87 cm and the shunt impedance are 120.3 and 93.1 MΩ/m, respectively. Hence, the cavity wall losses of the half-cell and full-cell is 0.12 and 0.84 MW, resulting in the cavity wall losses of the whole RF-gun as 0.96 MW.

3.6.2 Beam Power

For the experimental results describing in Chapter 6, an electron current of 1 A with kinetic energy of about 2.5 MeV can be generated from the RF-gun. Then, the beam power is simply estimated from production of beam energy and current as

$$P_{beam} \approx (E_{kin})(I_{beam}) = (2.5\ MeV)(1\ A) = 2.5\ MW. \tag{3.20}$$

Hence, the RF-power of about 2.5 MW is required to be supplied to the RF-gun for the beam loading. With both considerations for the cavity wall losses and for the beam loading, the RF-gun needs a total RF-power at least 3.5 MW for generating 1 A of 2.5 MeV electron beam. An RF-coupling coefficient of the RF-gun should be $\beta_{rf} \approx 1 + P_{beam}/P_{wall} = 3.6$. However, since the RF-power is applied into the RF-gun through an opening port at the full-cell coupling of the RF-power to the RF-gun depends on the RF-port opening size, the coupling ratio of the full-cell to the half-cell cell and individual electromagnetic properties of each cell.